A Comparison of Monte Carlo and Analytic Treatments of Displacement Damage in Si Microvolumes

C.J. Dale[1], L. Chen[2], P.J. McNulty[2], P.W. Marshall[1,3], and E.A. Burke[4]

1. Naval Research Laboratory, Washington, DC 20375-5345
2. Clemson University, Clemson, SC 29634-1911
3. SFA, Inc., Landover, MD 20785
4. Consultant

Abstract

In this paper, we compare Monte Carlo and analytic calculations of displacement damage resulting from inelastic proton reactions in Si. These comparisons include the nonionizing energy loss rate, the mean recoil damage energy spectra, and their associated variance. In the limit of bulk material, both approaches are in good agreement. As sensitive volumes shrink and incident proton energies increase, the ranges of the spallation recoil fragments approach the smallest dimension of the microvolume, and the pixel-to-pixel damage variance increases rapidly. In this regime, a Monte Carlo approach is used to describe the damage energy distribution. Indeed, we show that such simulations predict the 63 MeV proton-induced dark current histograms more accurately than present analytic methods.

The Monte Carlo code is also used to explore ground test fidelity issues for devices with small sensitive volumes.

I. INTRODUCTION

Solid state sensor arrays are increasingly being used in space for numerous applications including multispectral imaging, intersatellite communications, spectroscopy, and star tracking. Particle-induced degradation of charge coupled devices (CCDs) and charge injection devices (CIDs) can be dominated by displacement damage which increases the pixel dark current and degrades the charge transfer efficiency (CTE). It has been shown [1-6] that for devices with large numbers of small sensing volumes, it is critical to consider not only the mean damage, but also the distribution of the damage among the many pixels. High dark current pixels, caused by inelastic nuclear reactions occurring within the pixel, can interfere with low noise sensor applications. We note that for shielded space radiation environments, much of the displacement damage is caused by proton-induced inelastic events, also called spallation reactions. In [5], an analytic approach based on microdosimetry theory was developed to demonstrate that as the dimensions of a sensitive volume are reduced, the pixel-to-pixel damage variance increases significantly.

A different and complementary analytic method to predict the dark current distributions in sensor arrays was described in [6], and is based on calculations of the first and second moments of damage energy distributions from elastic collisions and nuclear reactions. These were incorporated into a model describing the probability of damage as a function of the proton energy and fluence, and the sensitive volume in Si. Comparisons in [6] between the predicted and measured leakage currents in Si CIDs illustrate how the Poisson distribution of higher energy nuclear reaction recoils affects pixel-to-pixel variance in the damage across the array. An underlying assumption in this approach is that there are few recoil trajectories that cross into or out of the microvolume (border crossers). That is, recoil damage in a sensitive volume is assumed to come only from recoils initiated and stopped within the volume. The excellent agreement between predictions and data for 12 and 22 MeV incident proton energies, suggested that the assumption was valid at these energies. However, the 63 MeV data exhibited less pixel-to-pixel variance than the model predicted. It was suggested in [2,6] that this occurred because the recoil ranges approached the smallest dimensions of the sensitive volume ($\approx$4.5 μm), resulting in border crossers. The probability of border crossing increases with increasing proton energy and decreasing sensitive volume. A new approach that accurately accounts for border crossers is the focus of this paper.

In this research, we develop Monte Carlo calculations to explore the conditions (as a function of sensitive volume geometry and incident particle energy) for which the analytic damage distributions are not adequate. The CUPID (Clemson University Proton Interactions in Devices) Monte Carlo code [7,8] is modified to evaluate the deposited displacement damage energy resulting from proton-induced spallation reactions [9]. We use this to compare the average recoil damage energies and nonionizing energy loss rates (NIEL) due to inelastic interactions as calculated by Burke and CUPID. The Appendix provides the Burke results for the mean recoil damage energy, its variance, NIEL, etc. in separate tables for the elastic and inelastic interactions.

In this paper, we use CUPID to examine three separate issues. First, damage distributions are calculated for a wide range of sensor geometries for a selection of proton energies from 12 to 250 MeV, and observed trends are discussed. Second, we investigate nonequilibrium displacement damage effects which occur when protons impinge on multilayered structures[12-14], and compare the results with experimental CTE data [14]. Third, the effect of the incident proton angle of incidence is evaluated for thin sensitive volumes.

0018-9499/94$04.00

II. COMPARISON OF ANALYTIC AND CUPID DISPLACEMENT DAMAGE CALCULATIONS

In this section, modifications to CUPID which allow the generation of the proton-induced displacement damage spectra associated with various sensitive volumes will be described and compared to the analytic calculation[5,10,11]. We emphasize damage from *inelastic* reactions. This is because elastic events generate recoils with energies about a thousand times smaller than inelastic reactions, leading to recoils with ranges much smaller than the dimensions of any sensitive volumes of practical interest. For this reason, it is not necessary to follow their trajectories in a Monte Carlo code. In addition, the variance in the elastic recoil damage energies is so small that the mean adequately characterizes the elastic contribution to the total damage energy deposited in a sensitive volume. The variance associated with the inelastic recoil spectrum, which is about 1000 times larger than the elastic variance [2,3], dominates the spread observed in the damage distributions.

A. CUPID Calculations of Displacement Damage

The CUPID Monte Carlo code has primarily been used to calculate the ionization energy loss in sensitive volumes for modeling of single event upset (SEU). The code successfully predicts proton-induced SEU rates from heavy ion data[15], and accurately predicts the charge collection spectrum in a SRAM [16]. Here, we compare CUPID displacement damage results with Burke's analytic calculation, which has been extensively compared to experimental results [2,5,6,10,12-14] and other calculations [17,18].

A detailed description of the physics underlying the CUPID model for inelastic (or spallation) reactions is given in [7,8]. Both CUPID and the analytic approach consider both the cascade and evaporation stages of a spallation event. In the initial cascade stage, the proton collides with a nucleon and initiates a chain of collisions which results in the ejection of some nucleons from the nucleus. The CUPID and Burke calculations are based in part on the work of Metropolis [19] for the intranuclear cascade though they differ in detail. The second stage of a spallation reaction is the evaporation part, during which nucleons are isotropically emitted in the center of mass frame. CUPID uses a so-called "liquid drop" model as described in [8], whereas Burke uses a Brownian motion model [13]. We note that because each stage is completed before the recoiling nuclear fragment has moved an appreciable distance, its momentum is determined by both processes. This "cascade-evaporation" model best characterizes proton inelastic collisions for energies between about 30-40 MeV and 500 MeV.

In CUPID, two nested volumes with identical shapes are specified; a large outer shell and a smaller inner volume referred to as the sensitive volume. Incident proton trajectories are normal to the pixel surface area, unless otherwise noted. For any spallation reaction in either the sensitive volume or outer shell, CUPID follows all recoil fragments from the point of production to the end of range. The code uses the angle and energy of the primary recoiling fragments to determine their final trajectory (i.e. does not consider secondary scattering). The vast majority of energy is deposited at the end of track. Straggling is not considered, nor is it relevant.

If a particle crosses the boundary of the sensitive volume, only the damage energy deposited in the sensitive volume is counted. The damage energy is calculated using the Lindhard partition [20]. An event is defined as occurring whenever a particle with $Z > 2$ enters the sensitive volume, or is generated within the sensitive volume. In effect, this means that only recoiling fragments are considered. Since the proton and alpha secondary particles contribute less than 10% to the bulk displacement damage (and usually less than 1%), the outer shell thickness is chosen to accommodate the $Z > 2$ recoiling fragment ranges, but not those for lighter secondary particles.

B. Comparison of CUPID with Analytic Results for the Mean Inelastic Damage Energy and NIEL

The Burke analytic calculation for the mean nonionizing energy loss rate (NIEL) [10-13] and the elastic variance at selected proton energies [5] have been described in detail elsewhere. The major improvements to the Burke calculation since 1986 and new values for the inelastic variance are summarized in Appendix A. In addition, the present values for NIEL, including the elastic and inelastic cross-sections and damage energies up to 1 GeV, are tabulated.

One important comparison to make between CUPID and the analytic method is their respective treatments of the *mean* inelastic recoil fragment damage energies versus incident proton energy, as shown in Figure 1. The CUPID calculations

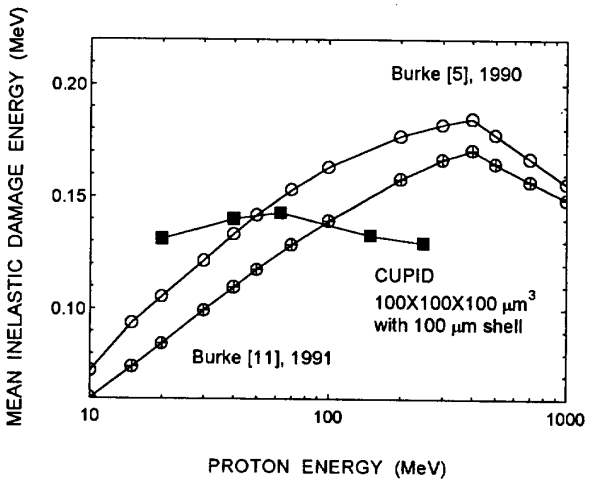

Figure 1 Comparison of inelastic damage energy calculations.

are for large sensitive volumes, and the outer shell is chosen to be thick enough to encompass the recoil fragment ranges in order to best approximate the bulk analytic results. This is assured by increasing the shell size until both mean and variance are insensitive to further changes.

The 1991 Burke results [11] are about 20% lower than the 1990 values [5] as described in Appendix A. For this type of calculation, agreement to within a factor of two is considered good, whereas CUPID and Burke agree to better than 35%, except at 20 MeV. The reduced agreement at the lower energies is not surprising since the codes use cascade-evaporation models which are less physically accurate below $\approx$ 30-40 MeV. Both of these calculations are also in good agreement with the HETC Monte Carlo calculations in [18]. The two Monte Carlo codes each show the decreasing trend in the mean inelastic damage energies with increasing proton energy above 70 MeV, although the recoil fragment populations have some differences. The primary reason for the divergence of the analytic calculation from the Monte Carlo codes above 100 MeV is the approximate treatment of the Lindhard partition in the analytic approach. In this case, the average recoil atomic number, Z, of the recoiling fragments is calculated, and then used in applying the Lindhard partition to the recoil spectra. As can be observed in the Tables, the distribution of Z broadens significantly as the proton energy increases from 63 to 150 MeV. The Lindhard partition is nonlinear with Z, and the error which arises from using a mean Z increases with proton energy. A smaller fraction of the total recoil energy goes into displacements for lower Z recoils, which explains the lower mean inelastic recoil energies obtained with CUPID and HETC.

The second major comparison to make between CUPID and the analytic calculation, is their respective predictions of the actual inelastic nonionizing energy loss *rate*. This quantity describes the mean damage energy deposited per gram of Si per unit proton fluence. It is useful for predicting experimental quantities like dark current increase histograms or charge transfer efficiency loss due to proton irradiation. To calculate this quantity, one has to consider the probability that an incident proton will have a spallation reaction. The analytic calculation uses an empirical expression for the inelastic cross-sections based on experimental results [21]. The nonionizing energy loss rate is then:

$$\text{Analytic Inelastic NIEL} = \left(\frac{N_o}{A}\right)\sigma_I \overline{E} \qquad (1)$$

where N_0 is Avogadro's number, A is the gram atomic weight, σ_I is the total inelastic cross-section, and $\overline{E}$ is the mean inelastic recoil damage energy.

The CUPID average damage energy loss rate is based on a large number of cases using Monte Carlo methods. A proton enters the Si with a randomly assigned impact parameter. If it strikes a nucleus, it is assigned a random mean free path based on the empirical relations for nucleon cross-sections given by Metropolis et al. [19] A collision occurs if the chosen path length, measured from the point of impact on the nuclear surface, does not carry the proton beyond the boundary of the nucleus. For a particular sensitive volume, we can define an effective inelastic "cross-section" as the number of events divided by the incident proton fluence. Recall that an event occurs when a Z > 2 particle (i.e. recoil fragment) crosses into, or else is generated inside the sensitive volume. In this case, the damage energy loss rate is

$$\text{CUPID Inelastic NIEL} = \left(\frac{1}{gSi_{S.V.}}\right)\frac{N}{\Phi}\overline{E}_{S.V.} \qquad (2)$$

where $gSi_{S.V.}$ is the total mass of the Si nuclei in the sensitive volume, N is the number of events, Φ is the incident proton fluence simulated, and $\overline{E}_{S.V.}$ is the average damage energy deposited in the sensitive volume.

Figure 2 shows the inelastic NIEL results of CUPID and both Burke calculations, which agree to within about 20%, except at 20 MeV. In the case of CUPID, calculations were performed for outer shell thicknesses from 4 to 100 μm, in

Table I : 63 MeV Protons on Si

Recoil Element	Average Damage Energy (MeV)	Fraction of Events	Average Range (μm)
P	0.137	0.00685	0.752
Si	0.137	0.121	0.348
Al	0.152	0.398	1.67
Mg	0.152	0.374	2.51
Na	0.138	0.0844	3.33
Ne	0.121	0.0109	4.14
F	0.0994	0.000821	4.55
O	0.0746	0.00396	6.47

Table II : 150 MeV Protons on Si

Recoil Element	Average Damage Energy (MeV)	Fraction of Events	Average Range (μm)
P	0.133	0.00395	0.785
Si	0.141	0.0872	0.233
Al	0.145	0.219	1.45
Mg	0.147	0.258	2.47
Na	0.137	0.213	3.61
Ne	0.118	0.129	4.88
F	0.0952	0.0293	6.15
O	0.0641	0.0368	8.33
N	0.0390	0.0180	11.8
C	0.0182	0.00466	22.4
B	0.00807	0.000819	23.5
Be	0.00377	0.000382	106

order to assure that any outflow of recoils from the sensitive volume was balanced by recoils entering the sensitive volume, that is, that recoil damage energy equilibrium conditions existed. As the incident proton energy increases, the lower Z fragments with longer ranges become more prevalent, as shown in Tables I and II. By 250 MeV, even a larger outer shell is required to obtain a good mean damage energy value. This makes the Monte Carlo technique extremely inefficient for the high proton energy calculations since a large fraction of the collisions are in the outer volume, and do not cross the sensitive volume to count as an event.

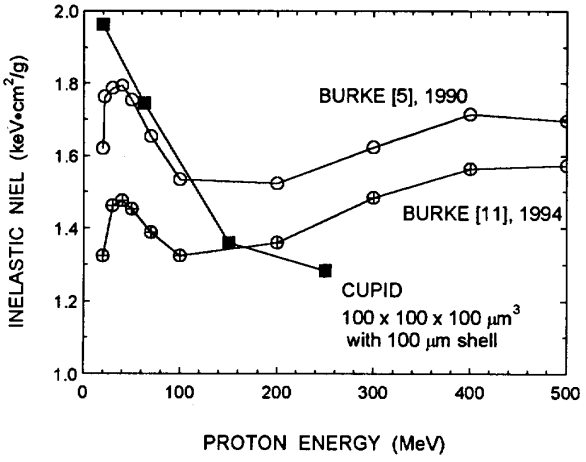

Figure 2 Comparison of NIEL results from Monte Carlo simulations for large senstive volumes and analytic calculations.

It would be interesting to generate a Lindhard correction function for the analytic calculation of the mean inelastic recoil energies, and then compare the respective inelastic NIEL results. The results would be in even better agreement at the higher proton energies. Any remaining differences would provide a comparison of the Monte Carlo cross-sections with the experimentally based cross-sections used in the analytic formulation. The reduced agreement at 20 MeV is partly due to the model limitations, as mentioned above. In addition, the determination of a suitable cross-section for the analytic calculation becomes more difficult near 20 MeV because the empirical formula used [21] is less valid and diverges somewhat from the experimental cross-section data. However, the accuracy of the inelastic contribution to NIEL at 20 MeV is not important since the elastic portion comprises 75% of the total NIEL at this proton energy. Experimental results must be compared with the total NIEL.

III. Comparison With CID Proton-Induced Dark Current Histogram

First we compare the calculated damage distributions with histograms of proton-induced dark current increases measured in charge integration device (CID) imagers as reported in [6]. To derive damage energy distributions, both CUPID and the analytic approach in [6] calculate the elastic and inelastic contributions, which are then combined. The cumulative damage distribution of multiple *inelastic* events is calculated using CUPID by introducing the spallation events randomly over a simulated 256x256 pixel array. The inelastic damage energy deposited in each pixel during the simulated 1.4×10^{11} cm^{-2} proton exposure is then summed, forming a array of pixel damage energies. The outer shell for each sensitive volume is 4 μm.

The CUPID simulation also reproduced the CID readout conditions in which the charge integrated under the row electrode (17x17x4.5 μm^3) 75% of the time, and under the column electrode (17x4x6.5 μm^3) 25% of the time. CUPID used the total elastic cross-section and mean damage energy values in [6] to calculate the elastic contribution to the damage energy in each pixel. This is reasonable because it is the inelastic interactions that dominate the damage energy variance as discussed in the introduction to Section II.

The result is shown in Figure 3, and compared to CID dark current data and the analytic prediction [6]. Both calculations of the damage distributions were normalized to the dark current data using the measured conversion factor of 2.2 nA/cm^2 per MeV as described in [6]. The mean damage energies of the two calculations agree to within 5%. Note that the Monte Carlo treatment of the displacement damage energy deposited, including recoil trajectories that cross the borders of the sensitive volume, is required for the observed close agreement with the dark current data, as suggested in [2,6]. This is because the recoil fragments have ranges that extend over a significant fraction of the depletion depth, as seen in Table I.

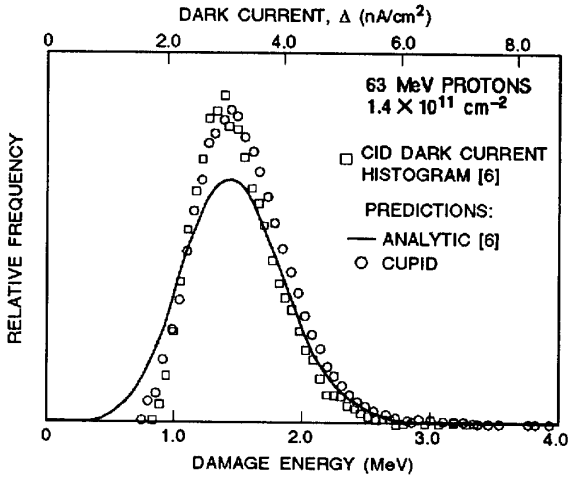

Figure 3 Analytic and Monte Carlo damage distributions are compared to a histogram of irradiation induced dark current increases in individual pixels.

For completeness, we observe that the variance in the observed dark current and associated simulated damage distributions is also highly dependent of the number of interactions (and its variance) that is observed for a given particle, fluence, and sensitive volume. This issue is explored in detail elsewhere [2,5,6,22]. In the case of the dark current spectrum shown in Figure 3, the proton fluence is high enough that on average there are 1400 elastic events in each pixel. The highest dark current pixels occur when up to 6 inelastic interactions occur in one pixel, but are only a factor of 3-4 from the mean because of the large elastic contribution in each pixel. Consider a low fluence such as $4x10^8$ cm^{-2}, that the CID might encounter early in a space mission. In this case, there would only be about 8 elastics per pixel, so a pixel with an inelastic event would have a damage energy almost a 1000 times greater. On average, one in 70 pixels would have a single inelastic event. By histogramming the damage energies in the pixels, we would create an "inelastic single event spectrum" to the extent we ignore the minuscule elastic contributions. It would be very interesting to acquire lower fluence "single event" data on imagers that do not exhibit high electric field effects [e.g. 5,6] to explore the dark current variance under these conditions.

IV. INELASTIC SINGLE EVENT DAMAGE DISTRIBUTION CALCULATIONS

In this section, single event damage distributions are calculated for microvolumes (or "pixels") representative of sensitive volumes for dark current generation in sensor arrays, except as noted. Of course, the techniques are more generally applicable to other device types with comparable sensitive volumes (e.g. a FET channel). The purpose of this section is to illustrate the dependence of the inelastic damage variance on microvolume geometry and incident proton energy. This enables one to recognize under what conditions the variance becomes very large, and when the Monte Carlo calculation is required to evaluate its magnitude.

As described in [2,5], the pixel-to-pixel variation in the damage energy deposited is well characterized using the concept of recoil relative variance, $(\sigma/\mu)^2$, where μ is the mean damage energy associated with the damage energy spectrum, and σ is the standard deviation. Single event spectra, such as the one shown in Figure 4, reflect the large variation in the damage energy of recoils produced by an incident particle of a given energy. The higher energy peak reflects recoils that have deposited most of their energy with in the volume. The lower energy events represent recoils that have crossed the sensitive volume boundary and stopped outside. These "crossers" are more dominant as the volume is reduced, and have a large effect on the relative variance. Almost all of the simulations presented here are derived from single event spectra representing at least 1000 events, and usually many more. A detailed examination of single event spectra appears in [22]. Single event spectra do *not* include the variation in the number of primary particle interactions occurring in a given volume for a certain particle fluence, which is included in multiple event spectra such as in Figure 3.

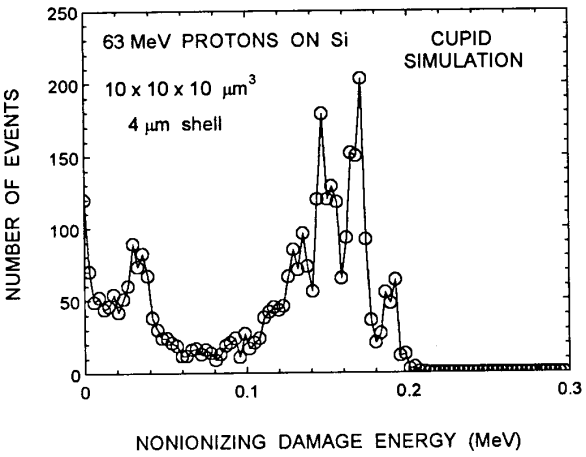

Figure 4 Single event inelastic recoil spectrum.

A. Inelastic Relative Variance vs Pixel Geometry

As Figure 5 illustrates, in the limit of large volumes, the Monte Carlo approach yields relative variance value close to the analytic "bulk" relative variance. The good agreement is particularly significant, since the variance is a more stringent test than comparison of just the mean damage energies. All Monte Carlo calculations were made with 4 μm shells, although many were repeated with 10 and 100 μm shells to verify that an adequately thick outer shell was used.

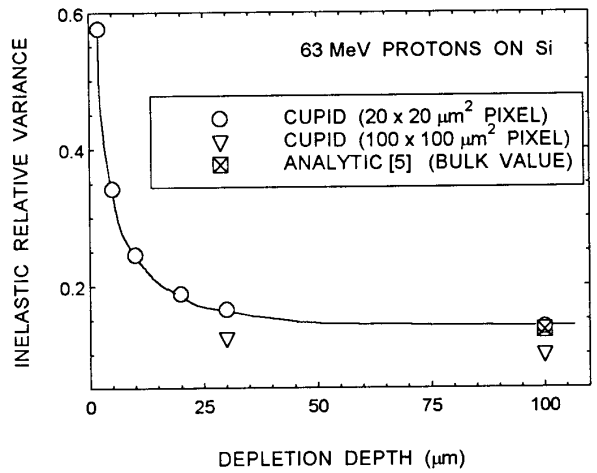

Figure 5 The recoil relative variance changes most rapidly in the regime where the recoil ranges are comparable to the depletion depth since this is when the relative importance of the crossing events is changing the most.

The important message from Figure 5 is that the relative variance increases sharply with decreasing depletion depth over a range relevant to device depths. This means that for many realistic device dimensions, it is critical to properly account for the displacement damage deposited in trajectories which cross a sensitive volume in order to evaluate the damage (or dark current) distributions.

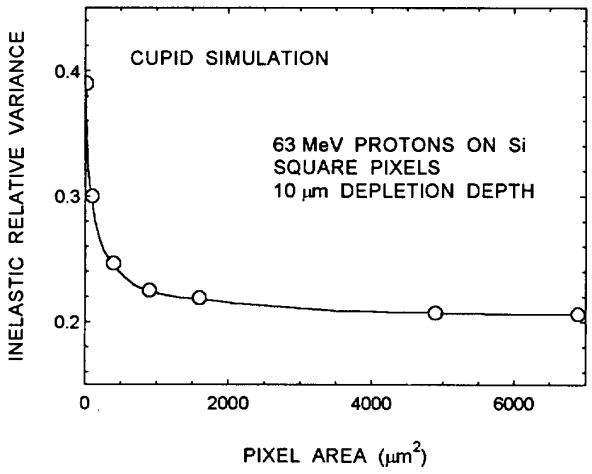

Figure 6 The recoil relative variance increases rapidly as the pixel area becomes very small.

Similar trends in the single event relative variance are observed as a function of pixel areas as illustrated in Figure 6. The reduction in relative variance with increasing area is less dramatic than for increases in the depletion depth, but is still a very strong function of area for the smaller areas. The relative variance is particularly sensitive to the depletion depth because of the forward directed nature of the inelastic recoils. This is an important point for interpreting test data since both dependencies must be understood to make space predictions with omnidirectional proton fluences.

B. Inelastic Relative Variance vs Proton Energy

Figure 7 shows the relative variance evaluated from CUPID single event spectra calculated for protons between 40 and 250 MeV incident on both a large sensitive volume, and on the same 17x17x4.5 μm^3 volume estimated for the CID dark current measurements. The much larger relative variance for the small volume results from the dominance of the crossing recoils such as those observed in Figure 4. The frequency of crossers increases as the proton energy increases and longer range recoils are produced. The crossing events significantly lower the mean deposited energy (especially for the lower Z recoils) and modestly increase the variance (5% effect), causing the relative variance to increase from 0.32 at 40 MeV to 0.59 at 250 MeV.

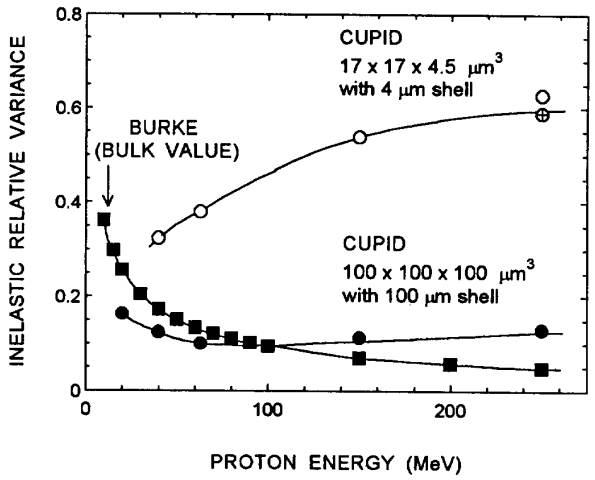

Figure 7 The magnitude and energy dependence of the recoil relative variance is very different for the bulk and small volume cases. The ⊕ value represents the value for a 10 μm shell which is required at 250 MeV to accommodate the longer recoil ranges.

The previous analytic relative variance calculations which are in good agreement with experimental CID dark current histograms at 12 and 22 MeV [5], have been extended to a wide range of proton energies. They are plotted as the solid squares in the figure and are in good agreement with the CUPID calculations for large volumes. As discussed in [5], the relative variance decreases with increasing proton energy even though the variance is increasing, because it is dominated by the rapid increase in the mean damage energy. Also, in the bulk case the mean is much larger than the associated standard deviation.

The rapid decrease in the bulk inelastic relative variance with increasing proton energy flattens at the higher energies because the mean damage energies saturate for a given Z as described by the Lindhard partition. The analytic calculation decreases relative to the Monte Carlo calculation primarily because the mean is underestimated in the analytic approach as discussed in Section IIB. However, the variance is also underestimated by the analytic calculation which assumes an average Z.

At high incident proton energies, the Monte Carlo calculation becomes less efficient because an increasingly thicker outer shell is required to contain all recoils that might contribute significantly to damage energy (and variance) of the inner sensitive volume. For the large volume, the relative variance increased by <2% as the shell thickness went from 10 to 100 μm for the 150 MeV case versus 34% for 250 MeV protons. As a result, it is not possible to say whether the small upturn in the relative variance at the highest proton energies is significant.

V. DISPLACEMENT DAMAGE SIMULATION FIDELITY ISSUES FOR SMALL SENSITIVE VOLUMES

The topics discussed in this section are concerned with the proper interpretation of ground based proton accelerator test results for use in making predictions of device performance in a trapped proton or solar flare environment.

A. Damage in Sensitive Volumes Near Interfaces

Discrepancies between NIEL and literature CTE values for proton energies above about 40 MeV have been observed and are described in [14]. There, it was proposed that displacement damage equilibrium of the forward directed recoils may not be achieved when higher energy protons are normally incident on a thin active volume located very near the surface, because the more energetic recoils deposit a significant fraction of their energy below the sensitive volume. This is also thought to be the cause of lower than expected GaAs JFET damage factors observed in [12,13].

This phenomena is analogous to the dose enhancement problem except that the role of secondary electrons is now replaced by recoiling nuclear fragments. The depth required to establish recoil damage energy equilibrium is determined by the ranges of these recoils.

CUPID was used to simulate the beam experiment by sending the protons normal to the 11 x 7 μm^2 pixel area. Figure 8 shows the inelastic damage energy deposited in the pixel per unit fluence assuming thicknesses of 0.15 and 1 μm. It takes several microns for damage energy equilibrium to be established. As expected, it is approached more quickly for the lower energy protons which produce recoils with shorter ranges. As the sensitive volumes become very small, the damage energies become dominated by events which occur outside the sensitive volume. In the case of the 0.15 μm thickness, the 4 micron shell was not adequate for 150 MeV protons and resulted in an underestimate of the deposited energy of ≈18%.

The sensitive volume thicknesses were chosen to simulate the CTE data. In the case of the EEV, Ltd. imagers in [14], the charge packet of less than 2000 electrons has been calculated to extend from a depth of ≈0.43 to 0.58 μm beneath the Si surface [23]. Larger charge packets will have significantly thicker sensitive volumes. It is difficult to estimate the equivalent Si thickness of the SiO_2 and polysilicon overlayers, but if we assume about a micron [24], we estimate about a 40% drop in the 150 MeV damage factor relative to the average NIEL whereas roughly an 60% lowering is observed. Considering the uncertainty in the data and overlayer estimate, this is reasonable agreement. No such effect is expected (or observed) in the 20 MeV data because the inelastics only provide ≈20% of the total damage energy.

When ground based data is used to make a prediction of device performance in space where it is exposed to an omnidirectional spectra behind shielding, the average NIEL energy dependence should be used. As shown in [25], for heavily shielded CCDs in a trapped proton environment, use of the energy dependence of the normally incident beam damage factors underestimates the CTE loss by a factor of two. State-of-the-art imagers are now being deployed with extremely thin overlayers (≈ 0.3 micron) designed to enhance the quantum efficiency [24]. In these cases, it is even more critical to consider the effects of recoil equilibrium when making a space prediction.

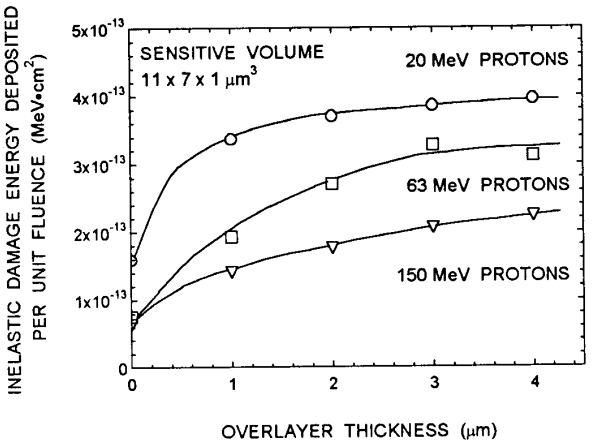

Figure 8a The approach to displacement damage equilibrium is displayed for several proton energies.

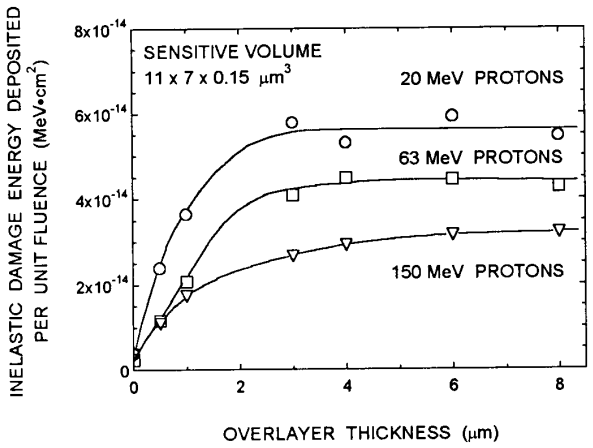

Figure 8b A thicker overlayer is required to reach damage energy equilibrium for the thinner sensitive volume.

B. Angle Dependence of Variance

The sensitivity of the relative variance to the proton angle of incidence for very thin volumes is investigated using CUPID. Assuming recoil equilibrium, the angle of incidence is

immaterial for the mean damage energy loss rate (NIEL), but the variance is dependent on the sensitive volume geometry. The 100 MeV CUPID simulations are performed as indicated in Figure 9 with 4 μm outer shells. As expected, the largest differences are between cases A and C, with B intermediate. For the 1 μm thick volume a 40% difference in the relative variance is found between A and C, but this difference increased to a *factor* of 4.4 for the 0.1 μm thick volume. It would be interesting to acquire data on the Kodak imager described in [9] which has an unusually thin dark current sensitive volume.

This simple "orthogonal angle" test can be used to decide whether a full omnidirectional calculation is warranted in order to perform space predictions of device performance. The CUPID code has been enhanced to perform this calculation for single event upset rates [26].

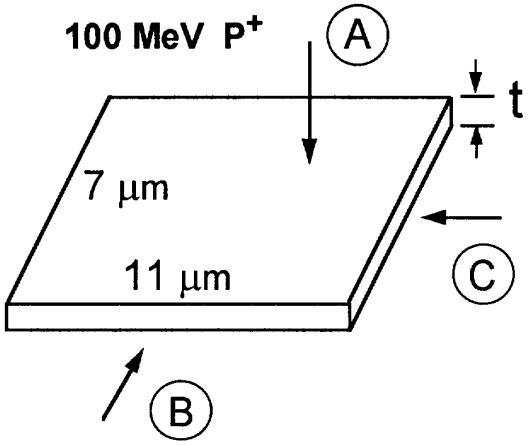

Figure 9 Schematic of the CUPID simulations at orthogonal angles.

VI. SUMMARY

The problem of pixel-to-pixel damage variation is important for modern sensor arrays. In this paper, we extend previous work by investigating the importance of treating the displacement damage energy contributions by proton-induced recoils which cross the boundaries of the sensitive volume using the Monte Carlo code CUPID. Excellent agreement is found between the CID dark current histograms at 63 MeV and the CUPID simulation.

Using the inelastic relative variance as a measure of the pixel-to-pixel variation in damage energy, we compare the CUPID results with previous analytic calculations which are extended to higher proton energies than previously reported. Both approaches show good agreement in the limit of bulk silicon. However, the regimes of microvolume geometry and incident proton energies for which the new Monte Carlo approach is necessary are clearly delineated. In the most general terms, the Monte Carlo approach is required whenever the recoiling fragments have ranges that are a significant fraction of the smallest sensitive volume dimension.

Finally, several displacement damage ground test fidelity issues are explored. The special case of displacement damage in thin sensitive volumes very close to the surface caused by normally incident protons is treated. We find that damage energy equilibrium may not be established until several microns below the Si surface. It is also noted that for some of the thinnest geometry sensitive volumes, the associated relative variance is a strong function of the angle of incidence of the incident protons. In these special cases, Monte Carlo codes can be used to make more accurate space predictions based on ground based accelerator data.

VII. ACKNOWLEDGMENTS

Partial support of this work by the Defense Nuclear Agency is greatly appreciated.

V. REFERENCES

[1] J.R. Srour, R.A. Hartmann, and K.S. Kitasaki, "Permanent Damage Produced by Single Proton Interactions in Silicon Devices," IEEE Trans. Nucl. Sci. NS-33 (6), 1597-1604 (1986).

[2] C.J. Dale, P.W. Marshall, E.A. Burke, G.P. Summers, and G.E. Bender, "The Generation Lifetime Damage Factor and its Variance in Silicon," IEEE Trans. Nucl. Sci. NS-36 (6), 1872-1881 (1989).

[3] P.W. Marshall, C.J. Dale, E.A. Burke, G.P. Summers, and G.E. Bender, "Displacement Damage Extremes in Silicon Depletion Regions," Ibid., 1831-1839 (1989).

[4] G.R. Hopkinson and Ch. Chlebek, "Proton Damage Effects in an EEV CCD Imager," Ibid., 1865-1871 (1989).

[5] C.J. Dale, P.W. Marshall, and E.A. Burke, "Particle-Induced Spatial Dark Current Fluctuations in Focal Plane Arrays," IEEE Trans. Nucl. Sci. NS-37 (6), 1784-1791 (1990).

[6] P.W. Marshall, C.J. Dale, and E.A. Burke, "Proton-Induced Displacement Damage Distributions and Extremes in Si Microvolumes," IEEE Trans. Nucl. Sci., NS-37 (6), 1776-1783 (1990).

[7] P.J. McNulty, G.E. Farrell, and W.P. Tucker, "Proton Induced Nuclear Reactions in Silicon," IEEE Trans. Nucl. Sci. NS-28 (6), 4007-4012 (1981).

[8] Peter J. McNulty, Wagih G. Abdel-Kader and Gary E. Farrell, "Proton Induced Spallation Reactions," Radiat. Phys. Chem., 43 (1/2), 139-149 (1994).

[9] L. Chen, P.J. McNulty, W.G. Abdel-Kader, T.C. Miller, and D.A. Thompson, "Single and Multiple Proton-Induced NIEL Events in Silicon," to be published in 1993 RADECS Conference Proceedings.

[10] E.A. Burke, "Energy Dependence of Proton-Induced Displacement Damage in Silicon," IEEE Trans. Nucl. Sci., NS-33 (6), 1276-1281 (1986).

[11] Edward A. Burke, "Radiation Hardening of Charge Coupled Devices," Final Report for NASA Goddard Space Flight Center Contract No. NAS5-31381, September 1991.

[12] E.A. Burke, C.J. Dale, A.B. Campbell, G.P. Summers, T. Palmer, and R. Zuleeg, "Energy Dependence of Proton-Induced Displacement in Gallium Arsenide," IEEE Trans. Nucl. Sci., NS-34 (6), 1220-1227 (1987).

[13] G.P. Summers, E.A. Burke, M.A. Xapsos, C.J. Dale, P.W. Marshall, and E.L. Petersen, "Displacement Damage in GaAs Structures," IEEE Trans. Nucl. Sci., NS-35 (6), 1221-1225 (1988).

[14] Cheryl Dale, Paul Marshall, Brent Cummings, Louis Shamey, and Andrew Holland, "Displacement Damage Effects in Mixed Particle Enviromnents for Shielded Spacecraft CCDs," IEEE Trans. Nucl. Sci., NS-40 (6), 1628-1637 (1993).

[15] J.M. Bisgrove, J.E. Lynch, P.J. McNulty, W.G. Abdel-Kader, V. Kletnieks, W.A. Kolasinski, "Comparison of Soft Errors Induced by Heavy Ions and Protons," IEEE Trans. Nucl. Sci., NS-33 (6), 1571-1576 (1986).

[16] P.J. McNulty, D.R. Roth. W.J. Beauvais, W.G. Abdel-Kader, and D.C. Dingo, "Comparison of the Charge Collecting Properties of Junctions and the SEU Response of Microelectronic Circuits," Int. J. Radiat. Instrum. Part D, Nuclear Tracks and Radiat. Meas. 19, 929-938 (1991).

[17] A. Van Ginneken, "Non Ionizing Energy Deposition in Silicon for Radiation Damage Studies," Fermi National Accelerator Laboratory Report FN-522, October 1989.

[18] M. Alurralde, M. Victoria, A. Caro and D. Gavillet, "Nuclear and Damage Effects in Si Produced by Irradiations with Medium Energy Protons," IEEE Trans. Nucl. Sci., NS-38 (6), 1210-1215 (1991).

[19] N. Metropolis, R. Bivins, M. Storm, A. Turkevich, J.N. Miller, and G. Friedlander, "Monte Carlo Calculations on Intranuclear Cascades," Phys. Rev. 110, 185-204 (1958).

[20] D.G. Doran, "Neutron Displacment Cross Sections for Stainless Steel and Tantalum Based on a Lindhard Model," Nucl. Sci. and Eng. 49, 130-144 (1972).

[21] J.R. Letaw, R. Silberberg and C.H. Tsao, "Proton-Nucleus Total Inelastic Cross-Sections: An Empirical Formula for E> 10 MeV," Astrophys. J. Suppl. 51, 271-276 (1983).

[22] L. Chen, P.J. McNulty, D.A. Thompson, T.L. Miller, and T.-H. Lee, "Dark Current Induced in Large CCD Arrays by Proton Induced Elastic Reactions and Single to Multiple Event Spallation Reactions," This Conference.

[23] A. Holland, "The Effect of Bulk Traps in Proton Irradiated EEV CCDs," NIM A326, 335-343, 1993.

[24] Private communication with Andrew Holland. The 2.5 μm overlayer estimate in [14] was too high.

[25] C.J. Dale and P.W. Marshall, "Displacement Damage in Si Imagers for Space Applications," Proc. SPIE, 1447, 70-86, 1991.

[26] R.A. Reed and P.J. McNulty, "Omnidirectional Proton Simulation Code Suitable for SEP Testing and Prediction of SEP Rates in Space," This Conference.

[27] P.W. Marshall, C.J. Dale, and E.A. Burke, "Proton-induced displacement damage fluctuations in silicon microvolumes," NIM B56/57, 847-850 (1991).

APPENDIX A

The original analytic NIEL calculation by Burke [10] has been improved in several ways since it was first published in 1986. In 1988, the spallation reaction model was modified to include the evaporation mechanism [13], although this did not make much difference in the Si case because of the Lindhard partition. In 1989 [2,3], the Lindhard correction was applied to the differential recoil spectrum instead of to the average recoil energy of the target atoms. In 1990 [5,6] new literature values were employed for the differential nuclear elastic cross-sections, and the inelastic cross-section for 22 MeV was reassessed in light of literature data. Finally, in 1991 [11], the inelastic reaction was investigated again. This resulted in new damage energies and average atomic numbers for the reaction products.

Tables III and IV tabulate the quantities required to calculate analytic damage distributions [6], NIEL and the relative variance for the elastic and inelastic cases. (The elastic variance may be found in [27] as a function of proton energy.)

Table IV : Parameters Describing Elastic Interactions for Protons on Silicon

Proton Energy	Cross Section	Damage Energy	Elastic NIEL	Nonelastic NIEL	Total NIEL
(MeV)	(barns)	(keV)	(keV•cm^2/g)		
1	18219	0.1578	61.86	--	61.86
1.5	12158	0.1621	42.4	--	42.4
2	9125.8	0.1647	32.35	--	32.35
3	6093.1	0.168	22.02	--	22.02
4	4576.9	0.1699	16.74	--	16.74
5	3667.2	0.1712	13.51	--	13.51
6	3060.6	0.1722	11.34	--	11.34
7	2627.4	0.1729	9.774	0.5164	10.29
10	1847.5	0.1784	7.091	0.7938	7.885
15	1241.0	0.1786	4.77	1.1389	5.909
20	937.7	0.2001	4.037	1.3235	5.36
30	634.5	0.2429	3.317	1.4613	4.778
40	482.8	0.275	2.857	1.4754	4.332
50	391.9	0.2884	2.432	1.4521	3.884
70	288.0	0.2861	1.773	1.3875	3.161
100	210.1	0.2814	1.272	1.324	2.596
200	119.3	0.2262	0.5808	1.3595	1.94
300	89.17	0.2168	0.416	1.4841	1.9
400	74.17	0.2158	0.3444	1.5633	1.908
500	65.20	0.2131	0.299	1.5723	1.871
700	54.97	0.204	0.2414	1.5434	1.784
1000	47.28	0.185	0.1882	1.4863	1.674

Table IV : Parameters Describing Inelastic Interactions for Protons on Silicon

Proton Energy (MeV)	Cross Section (barns)	Recoil Energy (MeV)	Recoil Damage Energy (keV)	Mean Atomic Mass No.	Recoil Variance $(keV)^2$	Nonelastic NIEL $(keV \bullet cm^2/g)$
7	0.4554	0.137	52.70	26.11	1106.71	0.5164
10	0.6127	0.196	60.21	25.95	1309.76	0.7938
15	0.7135	0.295	74.18	25.78	1638.33	1.1389
20	0.7275	0.394	84.55	25.66	1832.30	1.3235
30	0.6835	0.593	99.36	25.49	2018.59	1.4613
40	0.6253	0.792	109.65	25.37	2072.88	1.4754
50	0.5746	0.993	117.44	25.28	2069.85	1.4521
70	0.5016	1.395	128.55	25.15	1995.90	1.3875
85		1.700	134.52		1914.37	
100	0.4417	2.008	139.30	25.00	1831.51	1.324
150		3.044	150.83		1580.31	
200	0.4001	4.099	157.91	24.84	1423.43	1.3595
250		5.173	162.75		1272.44	
300	0.4142	6.266	166.42	24.73	1148.09	1.4841
350		7.379	169.66		1045.48	
400	0.4311	8.515	170.68	24.57	946.34	1.5633
450		9.673	168.40		831.44	
500	0.4437	10.85	164.68	23.77	694.50	1.5723
600		13.25	159.58		514.22	
700	0.4574	15.74	156.87	22.80	449.62	1.5434
850		19.67	152.94		369.36	
1000	0.4641	23.74	148.88	21.83	258.63	1.4863